An improved triangular form-based multiple flow direction algorithm for determining the nonuniform flow domain over grid networks

Pengfei Wu[1,2] Jintao Liu[1,2*] Xiaole Han[1,3] Meiyan Feng[1,2] Junyuan Fei[1,2]

[1]State Key Laboratory of Hydrology-Water Resources and Hydraulic Engineering, Hohai University, Nanjing 210098, China

[2]College of Hydrology and Water Resources, Hohai University, Nanjing 210098, China

[3]School of Earth Sciences and Engineering, Hohai University, Nanjing 210098, China

* Corresponding author. E-mail address: jtliu@hhu.edu.cn (J.T. Liu).

Key points

- A new multiple flow direction algorithm adopting the triangular facet division is developed to determine the dispersive flow paths.
- The flow is drained to triangular facets in the cardinal cells considering the nonuniformly-distributed flow domain over each grid.
- The new algorithm using the area split strategy can provide the most accurate total catchment areas and extracted flow paths.

Abstract

The naturally-existing diffusive flow makes the multiple flow direction (MFD) algorithm for digital elevation models with revisited values. However, owing to a generally accepted hypothesis, i.e., flow over a grid cell is uniformly distributed ignoring the micro-topography and the inflow direction/position, nearly no existing MFD algorithms can simultaneously force the flow along the exact dispersive path, and provide highly accurate hydrological/geomorphological parameters. In this study, an **i**mprovement **T**riangular **F**orm-based **M**ultiple Flow Algorithm called iTFM is proposed to limit the arbitrary dispersion caused by the conventional hypothesis through considering the nonuniform flow domain within a cell. In the new algorithm, each facet flow and its inflow direction/position are considered to route the flow along the local aspect over partial areas to downstream facets or cells. Facets with or without inflow can behave quite nonuniformly in contributing areas, namely flow domains. This procedure is adopted to generalize the nonuniformity and route the flow to the exact downstream facets. Quantitative assessments using artificial terrains show that iTFM suppresses the artificial dispersion effectively and extracts the flow paths highly

consistent with the exact ones. Compared with previous algorithms, iTFM provides the most accurate total contributing areas. In addition, vector split and area split strategies are compared for flow split within a facet which is a necessary step in both TFM and iTFM, and the results prove that area split is more efficient. Hence, it can be concluded that the iTFM algorithm combined with the area split strategy can better define the dispersion flow path.

Key words

Terrain analysis; Multiple flow direction; Dispersive flow path; Nonuniform flow domain.

1. Introduction

Surface flow paths describe the trajectories of transportation for the overland mass, including water, sediments and nutrient (Orlandini & Moretti, 2009; Zhou & Liu, 2002). The flow paths can provide several significant hydrological or geomorphological variables (Yamazaki et al., 2019), such as total contributing area (TCA; Kotyra et al., 2021; Nilsson et al., 2021), specific contributing area (SCA; Lindsay, 2003), topographic wetness index (TWI; Quinn et al., 1995), and stream power index (SPI; Moore et al., 1993). These variables are adopted as basic parameters by a wide range of studies, including relative saturation simulation (Beven & Kirkby, 1979), soil particle diffusion (Liu et al., 2013), landscape evolution (Bonetti et al., 2020), channelization mapping (Hooshyar et al., 2016), and prediction of soil properties (Moore et al., 1993). So the extraction of flow paths is a primary task for these mathematical models above (Shin & Paik, 2017).

From a physical perspective, the exact downslope flow path for a zero-dimension point source is a line that is perpendicular to contour lines everywhere when gravity is the only factor involved (Orlandini et al., 2014). This gravity-driven flow path is consistent with the definition of slope line (Bonetti et al., 2018; Maxwell, 1870), and its primary control is topography (Vivoni et al., 2005). However, it is impossible to store the real-world topography perfectly into a computer and calculate the flow paths independently for all points. All the mathematical models adopt numerical approximations of the topography and the grid digital elevation model (DEM) is used most widely (Li et al., 2021). The DEM discretizes a continuous terrain into a mass of grid cells, and the flow path is estimated for every cell (Wu et al., 2020). Besides, the flow originating from different points within a grid may reach different neighboring grid cells along respective slope lines owing to the grid structure and the micro-relief over soil surface (Costa-Cabral & Burges, 1994; Moore & Grayson, 1991). Hence, the flow path for a DEM cell should also be dispersed to multiple neighboring cells for a more realistic simulation.

To reproduce the dispersive domains of flow paths over the DEM, multiple flow direction (MFD) schemes assigning a cell with multiple drainage directions and presetting ratios for different downstream flows are widely adopted in scientific community (Freeman, 1991; Quinn et al., 1991). On the contrary, the single flow direction (SFD) algorithms route the flow to only one neighboring cell (e.g., Fairfield & Leymarie; 1991; Lea, 1992; O'Callaghan & Mark, 1984; Orlandini et al., 2003; Paik, 2008; Shin & Paik, 2017; Wu et al., 2020). MFD algorithms have been proven to outperform SFD algorithms by providing parameters varying smoothly and continuously (Wilson et al., 2007; Zhou & Liu, 2002). Thus, the MFD algorithm is worthy of development based on the application requirements, although the dispersion of flow paths is inconsistent with the physical definition of the drainage area (Maxwell, 1870; Tarboton, 1997).

The earliest MFD algorithms proposed by Quinn et al. (1991; QMFD) and Freeman (1991; FMFD) are based on the first SFD algorithm called D8 (O'Callaghan & Mark, 1984). While D8 diverts the flow across a cell to its steepest downslope neighboring cell, QMFD and FMFD distribute the flow to all downslope cells based on the slope gradient (Wilson & Gallant, 2000). However, these two algorithms can cause excessive artificial dispersion (Qin et al., 2007). Therefore, several other studies have attempted to modify the fixed-exponent coupled to the slope gradient in QMFD or FMFD and guide more flow to steeper cells (e.g., Holmgren, 1994; Qin et al, 2007). Another widely-accepted strategy to minimize the artificial dispersion called D∞ was introduced by Tarboton (1997), which divides a 3×3 window into eight planar triangular facets and directs the flow to at most two neighboring cells on the facet containing the steepest downslope direction.

D∞ is taken for a moderately dispersive algorithm (Orlandini & Moretti, 2009), and a consequently improved algorithm called MD∞ is proposed to address the weakness of D∞ by allowing multiple triangular facets to drain out the flow (Seibert & McGlynn, 2007). Similarly, another algorithm called Triangular Form-based Multiple (TFM) Flow Algorithm also accepts the triangular facet structure of D∞ (Pilesjö & Hasan, 2014). TFM considers the upstream-downstream relationship between different facets within a cell to determine the proportion of the flow distributed to eight facets, and drains the flow over every facet to its two downslope cells. TFM is proved to be one of the most accurate MFD algorithms by accuracy evaluation of SCA reproduction (Pilesjö & Hasan, 2014; Yan et al., 2018).

There remains a disadvantage that limits the accuracy of the MFD algorithms mentioned above, i.e., they assume all the flow over a cell is located at the cell center (e.g., FMFD, QMFD, D∞, MD∞) or covers the cell uniformly (e.g., TFM) at the beginning of distribution. The flow domain over a cell may not be uniformly distributed because the flow from every upstream cell may access from a short segment of the cell boundary and pass through only part of the current cell region (Cabral & Burges, 1994). Thus, points at different locations of a cell have different upstream domains. The neglect of this problem will

direct the partial flow to false downstream cells and lead to artificial dispersion. Several SFD algorithms take this problem into account and have made effective improvements (Orlandini et al., 2003; Shin & Paik, 2017; Wu et al., 2020). However, only a few methods try to solve the problem by MFD algorithms, including DEMON (Cabral & Burges, 1994) and D∞-LTD (Orlandini & Moretti, 2009). DEMON tracks the two-dimensional flow path from the current grid over the DEM based on the fitted aspect, but opposite directions between neighboring cells may appear (Tarboton, 1997). D∞-LTD adopts the transverse deviation between the cell center and inflow direction to adjust proportions of the flow to downslope cells for D∞, while this algorithm only shows a limited advantage to the existing MFD algorithms (e.g., Orlandini et al., 2012).

In this study, the authors introduce a newly developed MFD algorithm that can effectively limit the artificial dispersion by considering the nonuniform distribution of flow domain. The new algorithm named iTFM is an improved version of TFM. The rest of this paper is organized as follows. Section 2 proposes the theory and methodology of the iTFM algorithm. Section 3 presents the artificial terrains and the assessment criteria for quantitative accuracy assessments. Section 4 provides the results as well as discussions, and Section 5 introduces the conclusions.

2. Theory and methodology

2.1 Framework

iTFM is developed for DEMs without sinks and flats, so additional methods are required to remove sinks and flats firstly (e.g., Pan et al., 2012; Planchon & Darboux, 2002). Then all the cells are sorted into a queue in descending elevation order. In the algorithm, every cell (e.g., C_0 in Figure 1a) is sub-divided into eight triangular facets and the initial flow accumulation of every facet is set as 1/8 of the cell area. Finally, the flow distribution process is modeled for every cell in the queue with elevations from high to low.

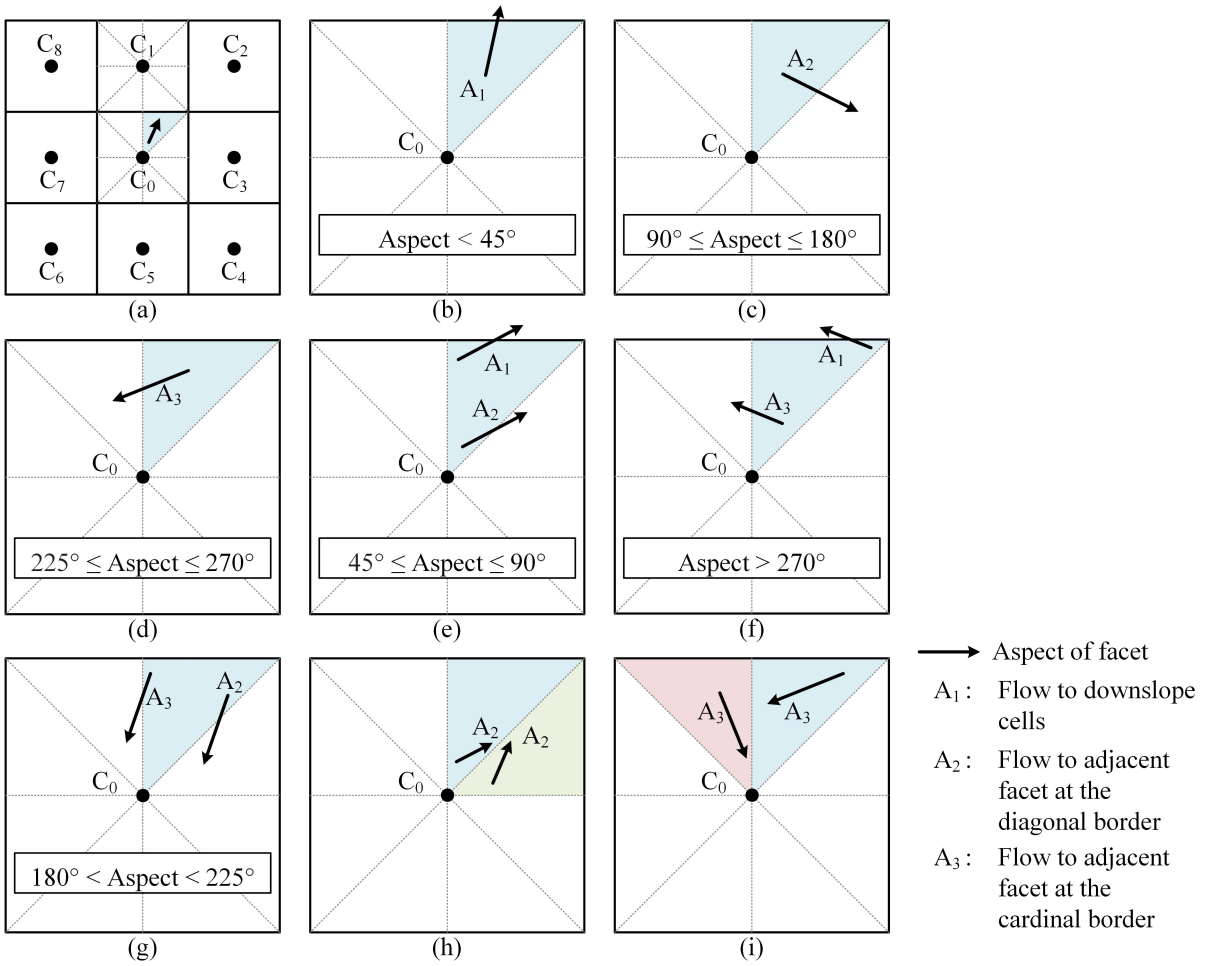

Figure 1. The scheme to distribute the flow within a cell is inherited from TFM. (a) A 3×3 window is adopted and the center cell is divided into eight triangular facets. The blue facet is selected for the illustration of the flow transport. The transport is based on the aspect of the current facet, with the cardinal and diagonal direction set as 0° and 45°, respectively. In some scenarios, the flow can be transported to (b) downstream cells or (c-d) one adjacent facet. In other scenarios, the flow is partitioned between (e-f) downstream cells and one adjacent facet, or (g) two adjacent facets. (h-i) If two facets slope towards each other, no transfer between these two facets will happen.

The blue facet of C_0 in Figure 1 is adopted for the illustration of the first part distribution process which happens within a cell, and this part of the process is inherited from TFM (Pilesjö & Hasan, 2014). The flow originating from different points in the current facet can reach the same border (Figure 1b-1d) or two borders (Figure 1e-1g) of the facet along the aspect, then the flow will

be drained out from the border(s). The flow (i.e., A_1) is drained to neighboring cells if it reaches the border coincident with the cell boundary, otherwise, it (i.e., A_2 or A_3) is drained to the adjacent facet in the same cell at the export border. There are three scenarios that the flow over a facet should be split into two parts for two targets (Figure 1e-1g), and two existing strategies based on the aspect for the split are discussed in Section 2.2. The process above is repeated for eight facets until all the flow is transported to neighboring cells.

When the flow routing within a cell is finished, one or more of the eight facets may drain the flow to neighboring cells. TFM adopts a strategy partly similar to D∞ and MD∞ that the flow out of a facet will be distributed to two cells adjacent to the current facet based on the slope gradient (e.g., C_1 and C_2 for the blue facet in C_0 in Figure 2, which is a partial enlargement of Figure 1). However, as shown in Figure 2a, if the flow over the blue facet moves along the aspect (the black arrow), all the flow can reach the cardinal neighboring cell (i.e., C_1) along the flow path (i.e., the yellow band) and a part of it can pass the cardinal neighboring cell and reach the diagonal neighboring cell (i.e., C_2) finally. So if the partial flow is distributed to C_2 directly according to TFM, the flow accumulation recorded for C_1 should be less than the actual value. Besides, if ignoring the nonuniform distribution of the flow domain over a downstream cell and distributing the flow equally to all the eight facets in the downstream cell following TFM, excessive artificial dispersion is observed (e.g., the green region in Figure 2b). In fact, the flow from an upstream facet to a downstream cell is received by only one facet in the downstream cell. For example, the grey facet in C_1 receives all the inflow from the blue facet in C_0 (Figure 2a). Based on the analysis above, all the flow to downstream cells out of a facet is added to the flow accumulation of its adjacent facet in the cardinal neighboring cell by iTFM. So when it comes to distributing the flow over a downstream cell, the flow rates over its eight sub-facet are different and it represents the nonuniform distribution of the flow domain over a cell in some measure. According to the scheme of iTFM, the flow over the blue facet in C_0 is distributed to fewer false regions as shown in Figure 2c. Hence, less artificial dispersion is caused by the nonuniform distribution hypothesis adopted by iTFM than the uniform one adopted by TFM. As can be noticed, although no flow is drained to C_2 by the blue facet in C_0 directly, partial flow is still transported to C_2 by the two facets owning red borders in C_1.

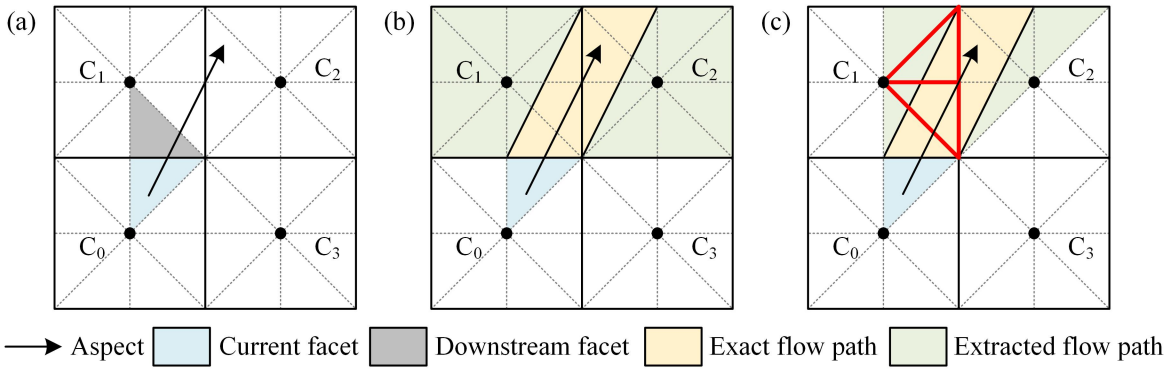

Figure 2. (a) An example for the analysis of flow distribution to downslope cells. All cells are on a planar plate so the aspect for every point is the same. The differences between the exact flow path and the extracted flow path for the blue facet by TFM and iTFM are shown in (b) and (c), respectively. A part of the extracted flow path is covered by the exact flow path.

Different from TFM, iTFM can be seen as a method entirely based on the triangular facet network because all the transport of flow occurs over the triangular facets. Moreover, compared to other algorithms which divide the DEM into a triangulated irregular network such as TFN (Zhou et al., 2011), iTFM is more efficient because the flow path for every cell should not be calculated independently and the computation over a cell happens only one time. The essential requirement for computations in iTFM is that eight times the memory space are required to store the flow accumulation for eight facets compared to traditional DEM-based algorithms.

Moreover, there is still a special case left that two adjacent facets sloping towards each other (Pilesjö & Hasan, 2014). In this case, if the neighboring cell at the direction of the adjacent line is higher than the current cell, the flow is stored into a temporary package and distributed to neighboring cells based on the final outflow proportion when other flow in the cell is drained (e.g., Figure 1i). Otherwise, the flow drained to each other is routed to the neighboring cell at the direction of the adjacent line, and then stored into the temporary package of the neighboring cell (e.g., Figure 1h). This step is a little different from Pilesjö and Hasan (2014). Generally, this special case can only happen to a handful of V-shape valleys, so the treatment has a slight impact on the results.

2.2 Strategies for flow split within a facet

In Figure 1e-1g, there are three scenarios that the flow should be sub-divided into two parts and drained to two different facets, i.e, when the facet aspect ranges from 45° to 90° (Figure 1e), from 180° to 225° (Figure 1g), and from 270° to 360° (Figure 1f). In previous studies, two usable aspect-based strategies that could be adopted for this task. The **v**ector **s**plit (VS; Pilesjö et al., 1998) strategy

and the **a**rea **s**plit (AS; Costa-Cabral & Burges, 1994) strategy are tested in this study. Both the strategies are included in the codes of TFM provided by Pilesjö and Hasan (2014) though only the VS strategy was introduced in their article.

While the VS strategy is adopted, the aspect of the facet (black arrows) is split into two vectors (green and violet arrows) as shown in Figure 3a-3c, and the flow distribution is proportional to the lengths (a and b) of the vectors (Pilesjö et al., 1998). For example, if the aspect value ranges from 45° to 90°, the aspect is split into one vector directing to 45° and one vector directing to 90° (Figure 3a). If the aspect value ranges from 270° to 360°, the aspect is split into one vector directing to 270° and one vector directing to 360° (Figure 3b). If the aspect value ranges from 180° to 225°, the aspect is split into one vector directing to 180° and one vector directing to 225° (Figure 3c). Then, the proportions (i.e., A_1, A_2 and A_3 in Figure 1) of flow distributed to different facets can be calculated according to the formulas in Figure 3. While the AS strategy is adopted, the aspect is used to divide the facet into two triangular regions at the intersection of two objectives (Figure 3d-3f). The flow is assumed to be distributed homogeneously over the facet, and all the flow in the same region can reach the same border and be drained to the same object along the aspect. So the flow distribution is proportional to the areas of the regions (i.e., S_1 and S_2 in Figure 3d-3f).

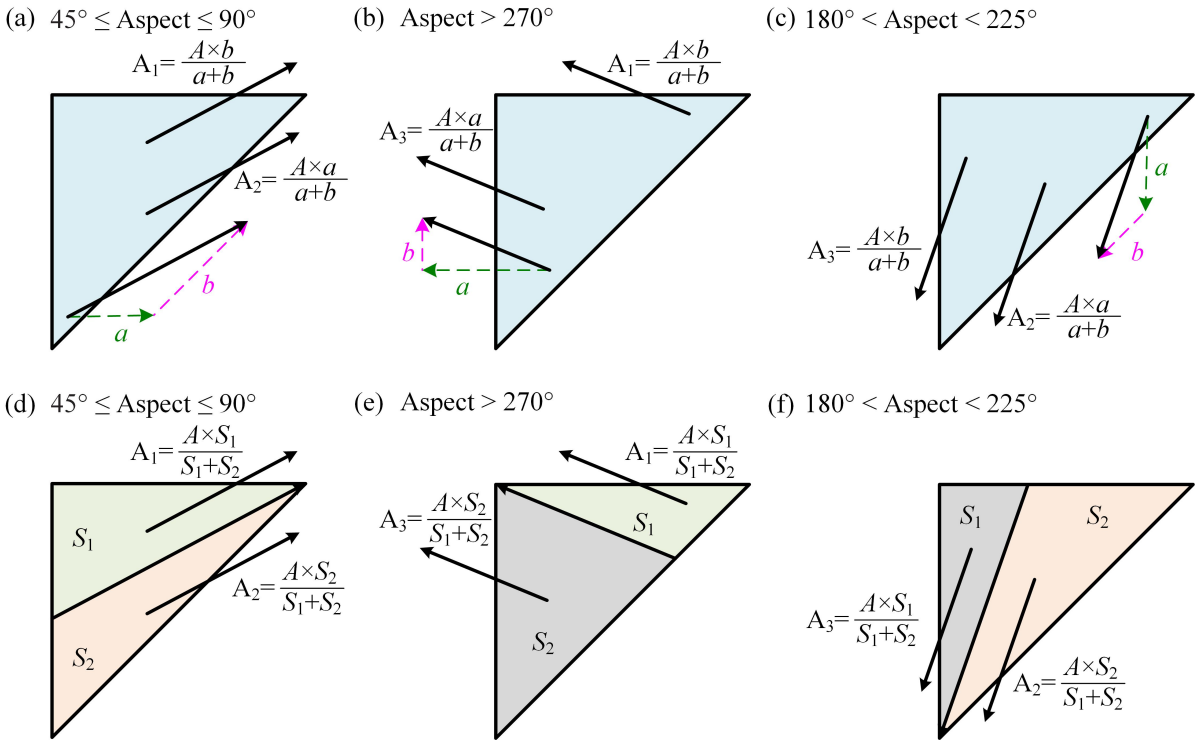

Figure 3. Examples of the flow rates drained to different facets using vector or

area split method. (a-c) The vector split (VS) method divides the aspect (black arrow) into two vectors (green and violet arrows), and the rates are decided by the length a and b of two vectors. (d-f) The area split (AS) method divides the facet into two triangles using a line paralleling the aspect, and the rates are decided by the area S_1 and S_2 of two triangles. In this figure, A is the total flow accumulation of the facet. A_1, A_2, and A_3 are flow accumulations drained to neighboring cells and adjacent facets as introduced in Figure 1.

Both VS and AS strategies can be applied to either TFM or iTFM framework. So combining different frameworks and split strategies, four algorithms are generated, which are named TFM-VS, TFM-AS, iTFM-VS, and iTFM-AS. Here TFM-VS is consistent with the original version of TFM proposed by Pilesjö and Hasan (2014).

3. Experiments

3.1. Artificial terrains

It is difficult to quantitatively assess flow direction algorithms using real-world DEMs because of the complex micro-topographical features (Wu et al., 2020). So artificial terrains are always adopted for assessments because the value of several topographic features can be obtained from their differentiable generation functions (Qin et al., 2013). Ellipsoid, inverse ellipsoid, plane and saddle are used most widely (e.g., Li et al., 2020, 2021; Pilesjö & Hasan, 2014; Zhou & Liu, 2002). Ellipsoid, inverse ellipsoid and plane represent divergent, convergent and plain terrains, respectively. And saddle is a complex combination of divergent and convergent terrains. In this study, these artificial terrains are adopted for quantitative assessment, and the formulas proposed by Li et al. (2021) are used to create them. Three-dimensional visualizations of these terrains are shown in Figure 4. Here we adopt the terrains with five different resolutions (1 m, 2 m, 5 m, 10 m, 20 m) to analyze the effect of the DEM resolutions on the accuracy of algorithms.

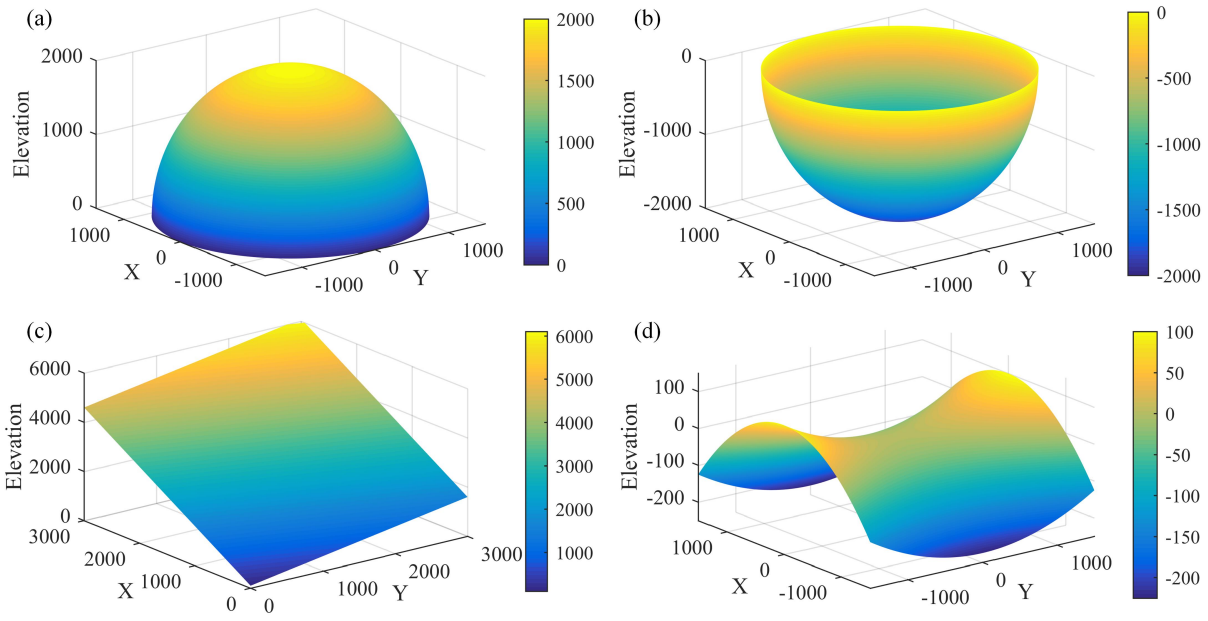

Figure 4. Four artificial terrains are used for the comparison between different algorithms, including (a) an ellipsoid, (b) an inverse ellipsoid, (c) a plane, and (d) a saddle.

3.2. Assessment methods and criteria

The performance of three existing MFD algorithms (i.e., D∞, FMFD, and MFD-md) and four algorithms mentioned in Section 2.2 are compared on the artificial terrains. D∞, FMFD, and MFD-md are selected because they are classical and widely adopted for comparison (Li et al., 2020, 2021). In addition, the SFD algorithms are also employed to show the difference between the SFD and the MFD algorithms, and the classical D8 as well as the iFAD8 algorithm proposed by Wu et al. (2020) is selected. All the algorithms adopted here are listed in Table 1.

Table 1. Characteristic of algorithms adopted for the accuracy assessment.

Algorithm	Type	Whether attempts to limit the artificial dispersion?	Origin
D8	SFD	Yes	O'Callaghan & Mark (1984)
iFAD8	SFD	Yes	Wu et al. (2020)
D∞	MFD	Yes	Tarboton (1997)
FMFD	MFD	No	Freeman (1991)
MFD-md	MFD	Yes	Qin et al. (2007)
TFM-VS	MFD	No	Pilesjö & Hasan (2014)
TFM-AS	MFD	No	Pilesjö & Hasan (2014)
iTFM-VS	MFD	Yes	Current study

Algorithm	Type	Whether attempts to limit the artificial dispersion?	Origin
iTFM-AS	MFD	Yes	Current study

Flow direction algorithms are always assessed by reproducing the theoretical SCA derived from artificial terrains (e.g., Pilesjö & Hasan, 2014; Zhou & Liu, 2002). The estimated SCA is a ratio of the estimated TCA extracted by flow direction algorithms and contour length (CL) which also affects the accuracy of the estimated SCA (Chirico et al., 2005; Li et al., 2021). Hence, a fairer criterion is to assess the capacities of different algorithms to reproduce the theoretical TCA directly. Theoretical TCAs for the ellipsoid, the inverse ellipsoid and the plane are easy to obtain (Costa-Cabral & Burges, 1994), and a method proposed by Li et al. (2021) to calculate the theoretical TCAs on the saddle is also employed here. The root mean square error (*RMSE*) and mean absolute relative error (*MARE*) are used to assess the deviations between the estimated and the theoretical TCAs. *RMSE* and *MARE* for a terrain owning n cells is calculated as

where RE_i is the relative error between the estimated and the theoretical values of the ith cell, $ETCA_i$ and $TTCA_i$ denote the estimated and the theoretical values of TCA of the ith cell, respectively.

In addition to the numerical accuracy of extracted attributes, the position accuracy of the extracted flow path is also worthy of consideration (Li et al., 2020). In this study, the position accuracy of downstream flow paths is adopted and assessed by a new criterion.

As shown by a 2×2 window in Figure 5a, the domain of DEM can be divided into four types of regions, denoted as R_1, R_2, R_3 and R_4 (Li et al., 2020). R_1 represents the region that belongs to both the exact and the extracted flow paths, R_2 represents the region that belongs to the exact but not the extracted flow path, R_3 represents the region that belongs to the extracted but not the exact flow path, and R_4 represents the region that belongs to neither the exact nor the extracted flow path. Different from Figure 2, to be consistent with the grid structure of DEMs, here the extracted path contains a whole cell if any facet in it is passed by the flow. Here the method to acquire exact flow paths over the selected artificial terrains was proposed by Li et al. (2020). If both the exact and the extracted flow paths for a cell (e.g., D_0) are delimited over a DEM (e.g., Figure 5b), the proportion of every cell belonging to every type of region can be calculated. Then, two metrics of errors (E_1 and E_2) are adopted to describe the ratio of the flow that deviated from the exact path and the ratio of the exact flow path not covered by the extracted path, respectively. The metrics are expressed as

where , , and denotes the fraction of the ith cell belonging to the region type R_1, R_2, and R_3. denotes the flow accumulation distributed to the ith cell from the source cell. The new optimal criterion for position error (*PE*) of the extracted

flow path for the source cell combines E_1 and E_2, and is expressed as

Both E_1 and E_2 range from 0 to 1, so PE also ranges from 0 to 1.

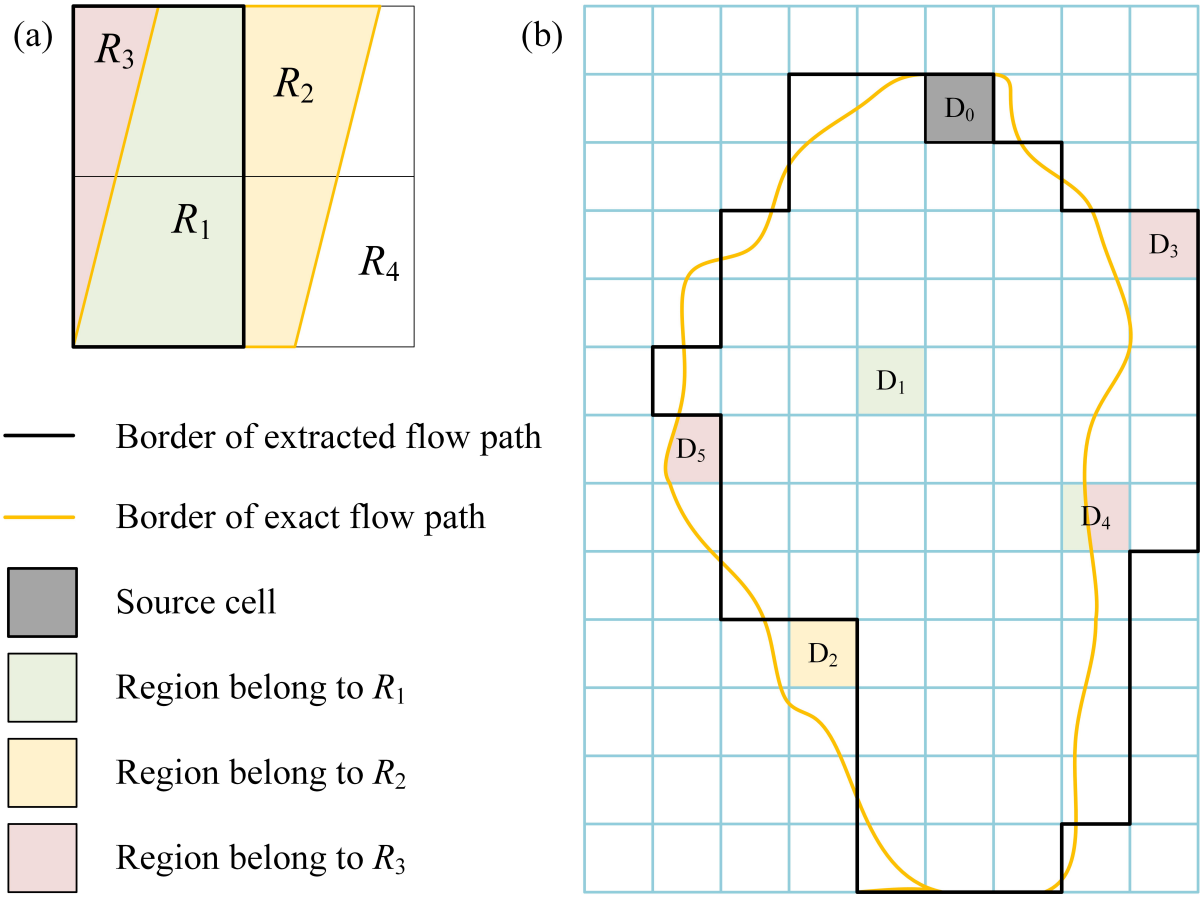

Figure 5. (a) A 2 × 2 window is used to show how to divide the DEM domain into four types of regions based on the exact and the extracted flow paths. This sub-figure is similar to the example of Li et al. (2020). (b) If the exact and the extracted flow paths are provided for a source cell (D_0), some DEM cells entirely belong to one region type (e.g., D_1, D_2 and D_3), and other cells belong to two types (e.g., D_4 and D_5).

4. Results and discussions

4.1. Deviations of estimated TCA

Figure 6 shows the spatial distribution of RE between the estimated and the theoretical 'true' value of TCAs over four artificial terrains with 1 m resolution. Both iTFM-VS and iTFM-AS have more cells with low REs (shown in bright

green) over any terrain than other algorithms. Especially, iTFM-AS seems to have the best performance with *RE*s ranging from -0.2 to 0.2 for nearly all cells. The results of TFM-VS and TFM-AS show fewer deviations than most selected existing algorithms (i.e., D8, iFAD8, D∞, and MFD-md) with fewer cells owing large *RE*s. Only FMFD has similar reasonable results with TFM-VS and TFM-AS. So far, it is still difficult to evaluate which split strategy (VS or AS) is preferred for the TFM algorithm according to the results in Figure 6. Compared with TFM-AS, TFM-VS has more cells with low values of *RE*s on the ellipsoid but high values of *RE*s on the inverse ellipsoid and the plane. The preference between the two algorithms is difficult for the evaluation on the saddle based on the visual assessment. In addition, the two selected SFD algorithms (D8 and iFAD8) have poorer performances than all the MFD algorithms with large-*RE* cells on most terrains. The reason for the chaotic spatial distributions of *RE*s by the SFD algorithms is that there is no consideration of dispersion.

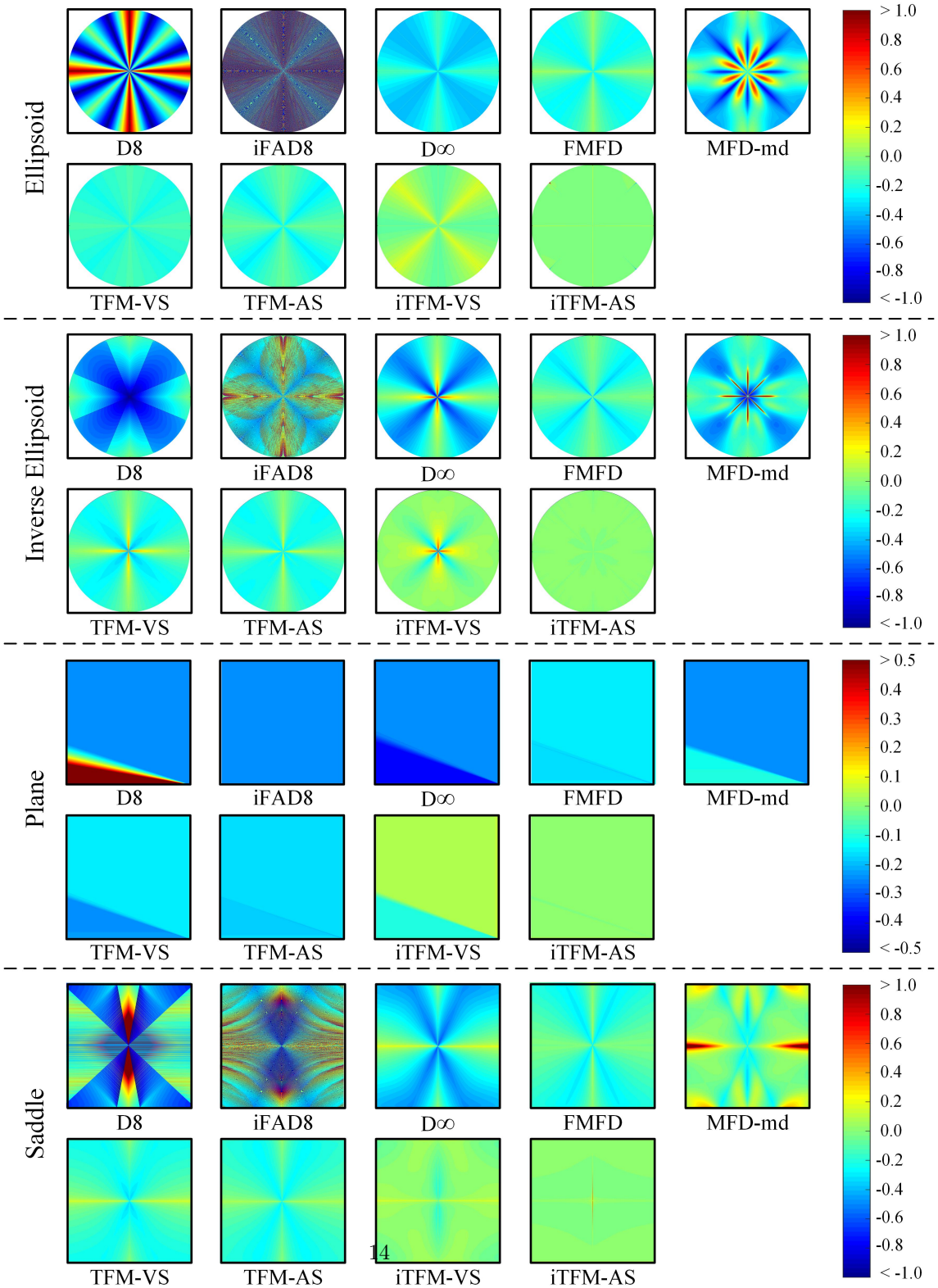
Ellipsoid
D8
iFAD8
D∞
FMFD
MFD-md
TFM-VS
TFM-AS
iTFM-VS
iTFM-AS
> 1.0
0.8
0.6
0.4
0.2
0.0
-0.2
-0.4
-0.6
-0.8
< -1.0
Inverse Ellipsoid
D8
iFAD8
D∞
FMFD
MFD-md
TFM-VS
TFM-AS
iTFM-VS
iTFM-AS
> 1.0
0.8
0.6
0.4
0.2
0.0
-0.2
-0.4
-0.6
-0.8
< -1.0
Plane
D8
iFAD8
D∞
FMFD
MFD-md
TFM-VS
TFM-AS
iTFM-VS
iTFM-AS
> 0.5
0.4
0.3
0.2
0.1
0.0
-0.1
-0.2
-0.3
-0.4
< -0.5
Saddle
D8
iFAD8
D∞
FMFD
MFD-md
TFM-VS
TFM-AS
iTFM-VS
iTFM-AS
> 1.0
0.8
0.6
0.4
0.2
0.0
-0.2
-0.4
-0.6
-0.8
< -1.0

Figure 6. The spatial distribution of relative errors (*RE*s) between the estimated and the theoretical TCAs by different algorithms over four artificial terrains with 1 m resolution.

For quantitative assessment, DEMs with five resolutions (1 m, 2 m, 5 m, 10 m, 20 m) are adopted. *RMSE*s and *MARE*s between the estimated and the theoretical TCAs with different algorithms and resolutions are shown in Figure 7. For most algorithms, *RMSE* increases linearly as the resolution value increases, and *MARE* is relatively steady. Although the *MARE* of iTFM-VS (brown line) or iTFM-AS (red line) seems to continuously increase with the resolution value increasing, their *MARE*s are always a small value which are smaller than 0.10 for all terrains. In most cases, iTFM-AS has both lower *RMSE* and *MARE* values than iTFM-VS, and the errors of iTFM-VS are lower than other algorithms. The only exception is that iTFM-VS has higher *RMSE*s than FMFD, TFM-VS and TFM-AS on the inverse ellipsoid (Figure 7c), though it has lower *MARE*s (Figure 7d). This phenomenon indicates that iTFM-VS has a poor performance at the bottom of the inverse ellipsoid, where both the theoretical and the estimated values of TCA as well as the *RE*s of the cells are high (see in Figure 6). In addition, the differences of *RMSE*s or *MARE*s between iTFM-VS and iTFM-AS are decreasing with an increasing resolution value, but iTFM-AS is still more accurate in most cases when the resolution reaches 20 m. TFM-VS has slightly higher *RMSE*s than TFM-AS on the inverse ellipsoid (Figure 7c) and the saddle (Figure 7g) but slightly lower *RMSE*s on the ellipsoid (Figure 7a) and plane (Figure 7e). *MARE*s by TFM-AS are slightly lower than TFM-VS on all four terrains with most resolutions (Figure 7b, 7d, 7f and 7f). Hence, it seems that the AS strategy is a better choice than the VS strategy for the TFM algorithm, but the accuracy difference between these two strategies is small. For other existing algorithms, FMFD has a similar performance with TFM-VS and TFM-AS, while D∞ and MFD-md generally have worse performances. Consistent with the result in Figure 6, D8 and iFAD8 are the worst choices with the highest *RMSE*s and *MARE*s in most cases.

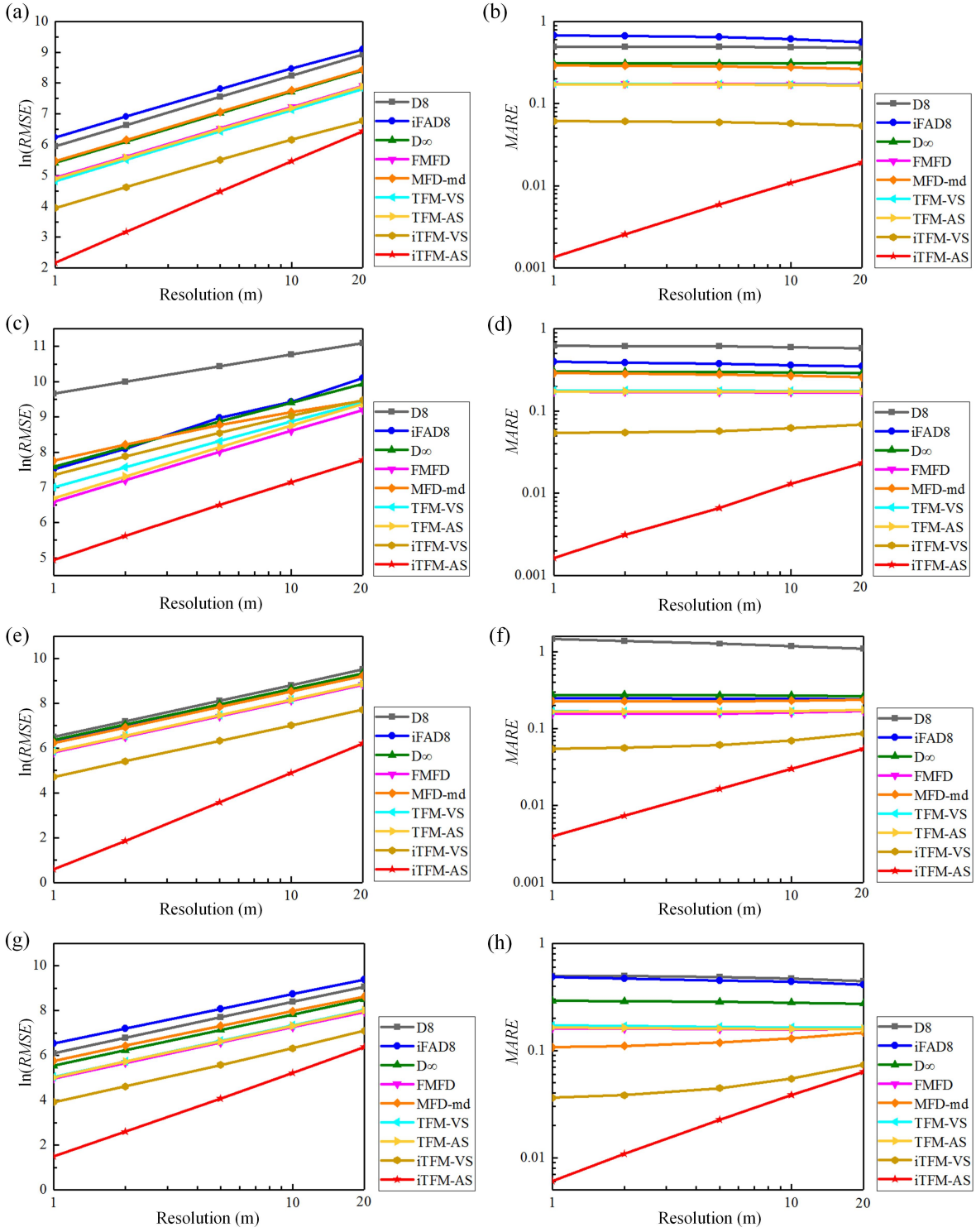
(a)
ln(RMSE)
Resolution (m)
(b)
MARE
Resolution (m)
(c)
ln(RMSE)
Resolution (m)
(d)
MARE
Resolution (m)
(e)
ln(RMSE)
Resolution (m)
(f)
MARE
Resolution (m)
(g)
ln(RMSE)
Resolution (m)
(h)
MARE
Resolution (m)
D8
iFAD8
D∞
FMFD
MFD-md
TFM-VS
TFM-AS
iTFM-VS
iTFM-AS

Figure 7. The root mean square error (*RMSE*) and the mean absolute relative error (*MARE*) of estimated TCAs derived by different flow direction algorithms on (a-b) the ellipsoid, (c-d) the inverse ellipsoid, (e-f) the plane, and (g-h) the saddle with six different resolutions. To show the difference between *RMSE*s more clear, its logarithmic value ln(*RMSE*) is adopted in the figure.

According to the results shown in Figure 6 and Figure 7, the iTFM framework (including iTFM-VS and iTFM-AS) is a better choice than the TFM framework (including TFM-VS and TFM-AS) for TCA estimation. The AS strategy is proven to have a better performance than the VS strategy for both TFM and iTFM frameworks when routing the flow over the triangular facets in a cell, although the accuracy enhancements from AS to VS are not remarkable for TFM. Here TFM-VS and TFM-AS show no obvious advantage to FMFD, which is inconsistent with the conclusions of Pilesjö and Hasan (2014) who fulfilled the assessments using SCA. Similar to the conclusion of Li et al. (2021), this difference is mainly caused by the errors of estimated CLs.

4.2. Position accuracy of extracted flow paths

PE in equation (6) can be calculated for every cell over all the artificial terrains. But due to the high computing runtime costs, only the 20 m-resolution DEMs are adopted to show the spatial distribution of *PE*s as well as several extracted flow paths. Then, the effects of the resolutions on the *PE*s by different algorithms are evaluated using the mean *PE* of several representative cells.

Figure 8 shows the spatial distribution of *PE*s between the extracted and the exact flow paths over four artificial terrains with different algorithms. D8 has the worst performance over all terrains with most cells' *PE*s higher than 0.5, while iFAD8 has a better performance than D8. This result arises because flow paths of iFAD8 are close to exact slope lines out from cell centers, while D8 provides the flow paths deviating from the exact slope lines seriously (Wu et al., 2020). So the flow path by iFAD8 is more possible to be a part of the theoretical flow path rather than the path by D8. Within all the selected MFD algorithms, FMFD, TFM-VS and TFM-AS have similar bad performances with high *PE*s in a mass of cells. This is owing to the effect of artificial dispersion. MFD-md limits the artificial dispersion by routing more flow to steeper downslope cells, so it has a slightly better performance in position accuracy. Meanwhile, the spatial distributions of *PE*s by D∞, iTFM-VS and iTFM-AS are similar, and show that position accuracies of these algorithms are higher than the accuracies of other algorithms. To show the consistency between the extracted and the exact flow paths in detail, several representative cells are selected for visual comparison in Figure 9-12. In these figures, cells are dyed with blue according to the flow rate received from source cells. So all the blue regions are cells covered by extracted flow paths out from the sources. And the dark blue regions are cells receiving the main part of the flow and can be regarded as the main stream. Moreover, exact flow paths are enveloped by red lines, and the *PE* for every extracted flow path is labeled.

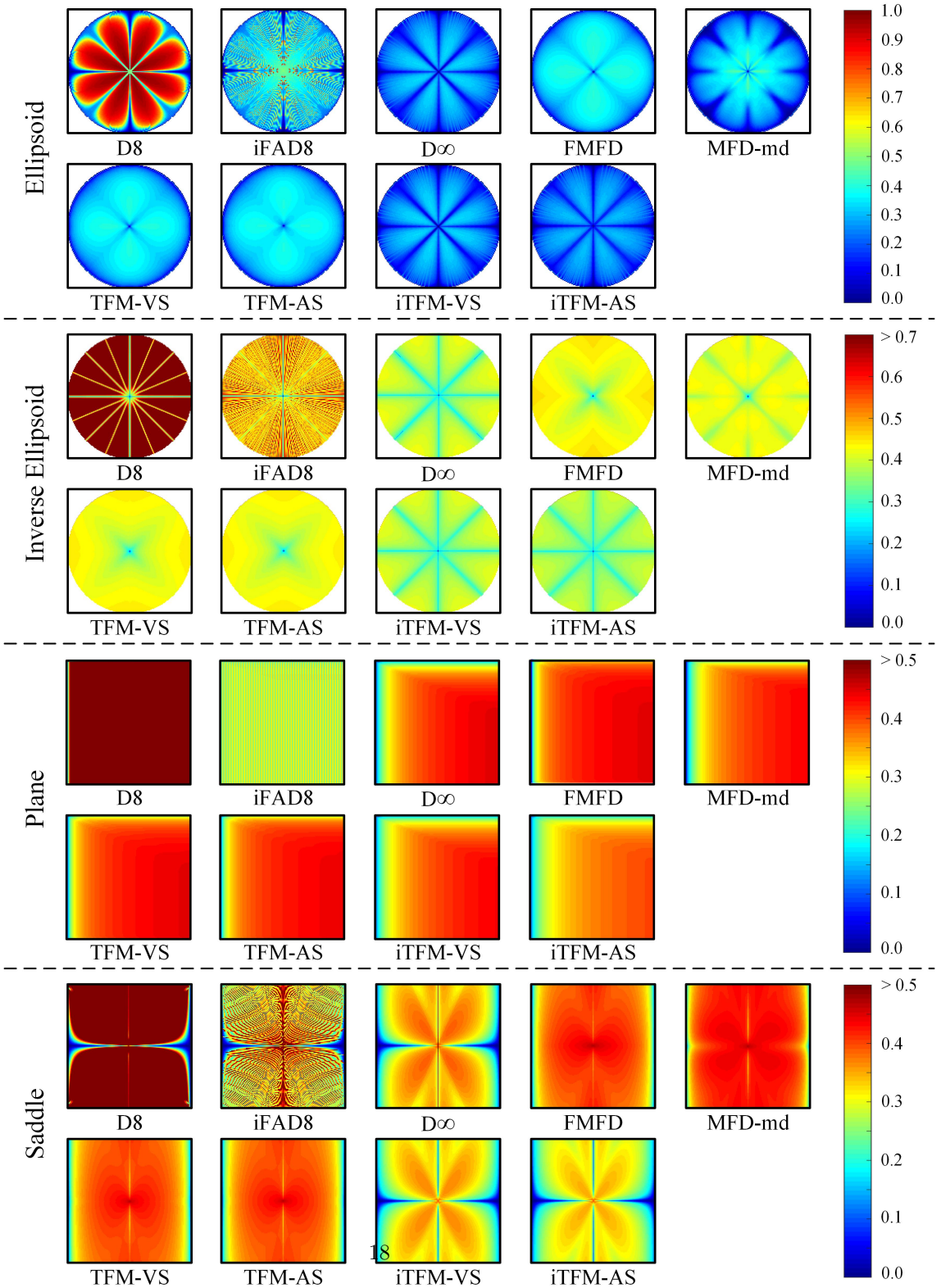
Ellipsoid
D8
iFAD8
D∞
FMFD
MFD-md
TFM-VS
TFM-AS
iTFM-VS
iTFM-AS
1.0
0.9
0.8
0.7
0.6
0.5
0.4
0.3
0.2
0.1
0.0
Inverse Ellipsoid
D8
iFAD8
D∞
FMFD
MFD-md
TFM-VS
TFM-AS
iTFM-VS
iTFM-AS
> 0.7
0.6
0.5
0.4
0.3
0.2
0.1
0.0
Plane
D8
iFAD8
D∞
FMFD
MFD-md
TFM-VS
TFM-AS
iTFM-VS
iTFM-AS
> 0.5
0.4
0.3
0.2
0.1
0.0
Saddle
D8
iFAD8
D∞
FMFD
MFD-md
TFM-VS
TFM-AS
iTFM-VS
iTFM-AS
> 0.5
0.4
0.3
0.2
0.1
0.0

Figure 8. The spatial distribution of position errors (*PE*s) between the extracted and the exact flow paths by different algorithms over four artificial terrains with 20 m resolution.

Flow paths for three cells (P_1, P_2 and P_3) over the ellipsoid extracted by different algorithms are shown in Figure 9. D8 and iFAD8 provide one-dimensional flow lines without dispersion (Figure 9a-9b). Especially, D8 provides an obvious false path for the cells which are not in the cardinal or the diagonal direction to the ellipsoid tip (e.g., P_3). Too many cells not belonging to the exact flow paths receives flow from the source cell when FMFD, MFD-md, TFM-VS or TFM-AS is employed (Figure 9d-9g), but FMFD, TFM-VS, and TFM-AS can drain most of the flow in the directions of theoretical flow paths. D∞, iTFM-VS, and iTFM-AS drain the flow to fewer cells than other MFD algorithms (Figure 9c, 9h-9i), which proves that D∞, iTFM-VS and iTFM-AS limit the artificial dispersion more effectively. However, D∞ provides a false one-dimensional flow line for P_2 in Figure 9c, and cannot make the main stream following the exact flow paths. iTFM-VS and iTFM-AS guide most of the flow to the regions of the exact flow paths, and iTFM-AS seems to have a better performance than iTFM-VS for P_3 by providing a feasible main stream that is symmetrical for the exact flow path. Flow paths by iTFM-VS and iTFM-AS are most accurate with the *PE* for every selected cell not higher than 0.30. iTFM-VS causes the lowest *PE* for P_2 while iTFM-AS causes the lowest *PE*s for P_1 and P_3. In addition, FMFD, TFM-VS, and TFM-AS are also relatively applicative with *PE*s for all selected paths not exceeding 0.40.

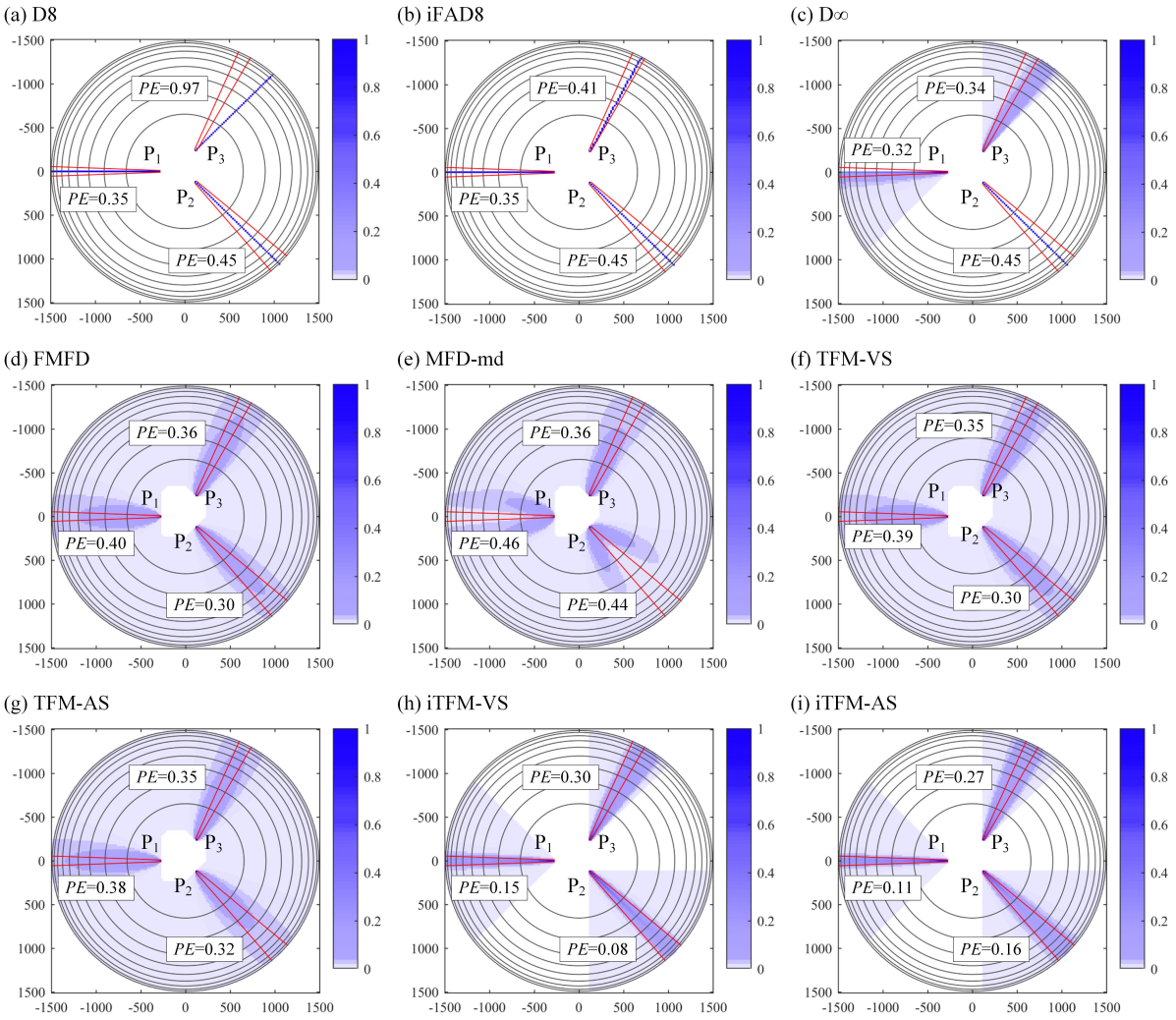

Figure 9. Extracted flow paths by different flow direction algorithms for three cells over the ellipsoid. Shades of blue represent the proportions of flow out from the source cell distributed to current cells. Contour lines have an interval of 200 m. The coordinates of selected source cells are P_1 (-280, 0), P_2 (120, 120), and P_3 (120, -240).

Figure 10 shows the extracted flow paths for the three cells, namely P_4, P_5 and P_6, over the inverse ellipsoid. There is little dispersion for the theoretical flow paths over the inverse ellipsoid, so nondispersive SFD algorithms are considered to be suitable for this terrain (Shin & Paik, 2017; Wu et al., 2020). However, both D8 and iFAD8 extract flow paths inconsistent with the exact flow path for P_6 (Figure 10a-10b). FMFD, MFD-md, TFM-VS, and TFM-AS identify

a mass of cells as false portions of flow paths (Figure 10d-10g). Compared to FMFD, TFM-VS and TFM-AS, the main streams of flow paths by MFD-md are narrower and more converged to the regions of the exact flow paths. D∞, iTFM-VS and iTFM-AS still have the best visual results that only the cell not in the cardinal or the diagonal direction of the ellipsoid tip (i.e., P_6) drains to excessive regions (Figure 10c, 10h-10i). The lowest *PE* equal to 0.25 for P_4 can be provided by D8, iFAD8, D∞, iTFM-VS and iTFM-AS. The lowest *PE*s for P_5 and P_6 are provided by D∞ and iTFM-AS, respectively. The *PE*s for extracted flow paths by D∞, iTFM-VS and iTFM-AS are close to each other and more accurate than other algorithms. TFM-VS and TFM-AS have similar performances which are worse than MFD-md.

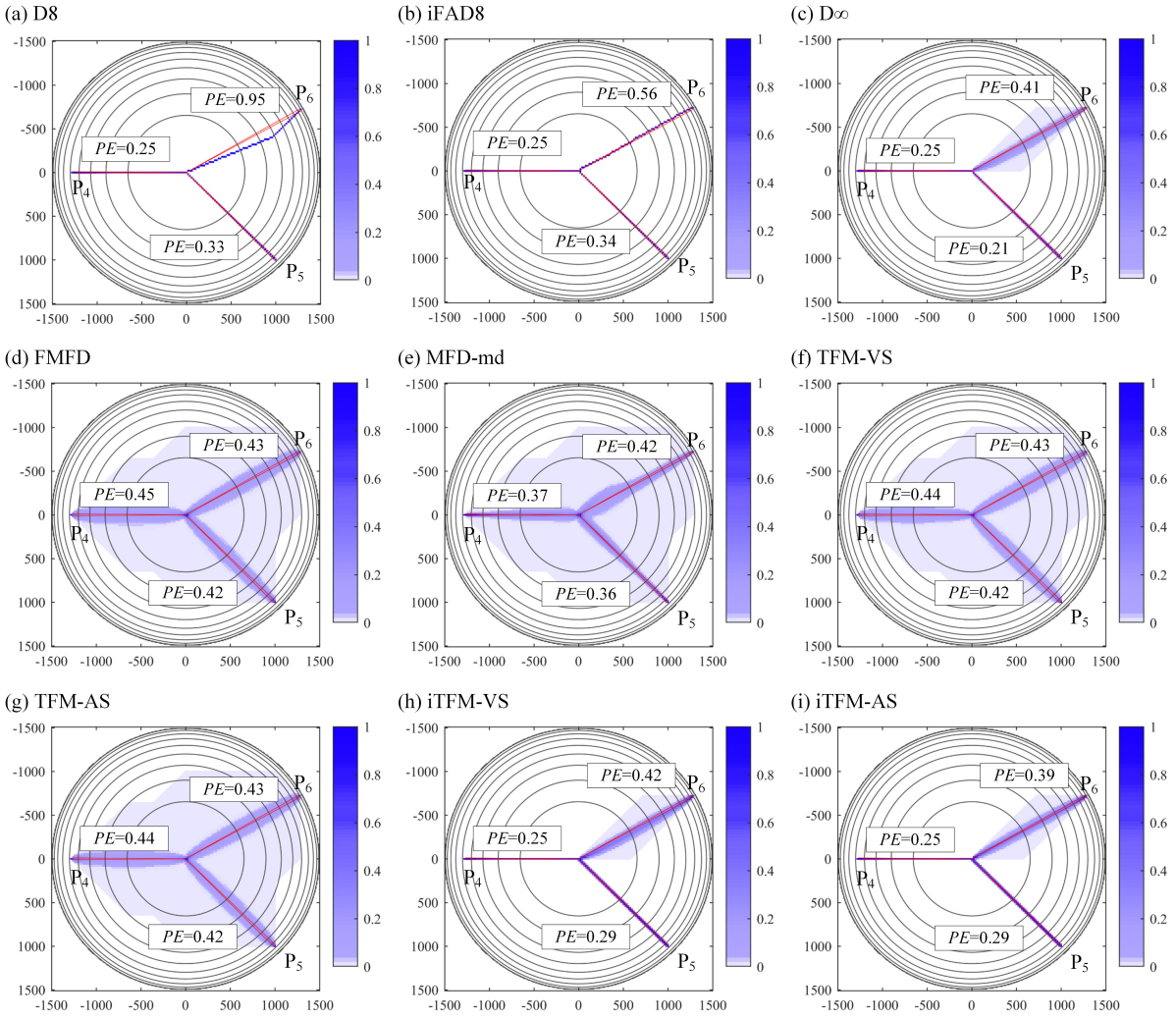

Figure 10. Extracted flow paths by different flow direction algorithms for three cells over the inverse ellipsoid. Shades of blue represent the proportions of flow out from the source cell distributed to current cells. Contour lines have an interval of 200 m. The coordinates of selected source cells are P_4 (-1280, 0), P_5 (1000, 1000), and P_6 (1280, -720).

The extracted flow paths for three selected cells (P_7, P_8 and P_9) over the plane are shown in Figure 11. There is little dispersion over the plane, and the nondispersive iFAD8 extracts reasonable flow paths along the exact flow paths (Figure 11b). The *PE*s by iFAD8 for these three cells are lower than any other algorithms. Meanwhile, D8 drains flow to the direction deviating from the theoretical direction (Figure 11a), because D8 does not consider the deviations between the selected direction and the theoretical direction (Wu et al., 2020). All the MFD algorithms produce excessive artificial dispersion on the plane, but the extracted flow paths by D∞, iTFM-VS and iTFM-AS cover fewer regions than the paths by FMFD, MFD-md, TFM-VS and TFM-AS (Figure 11c-11i). The main streams of flow paths by iTFM-AS take the exact flow paths as centerlines, which is more reasonable than D∞ and iTFM-VS. Within all the MFD algorithms, the *PE*s by iTFM-AS are lowest for all selected cells, and the *PE*s by iTFM-VS are only worse than iTFM-AS. Furthermore, TFM-VS and TFM-AS show no advantages over other algorithms except D8 according to the *PE* values.

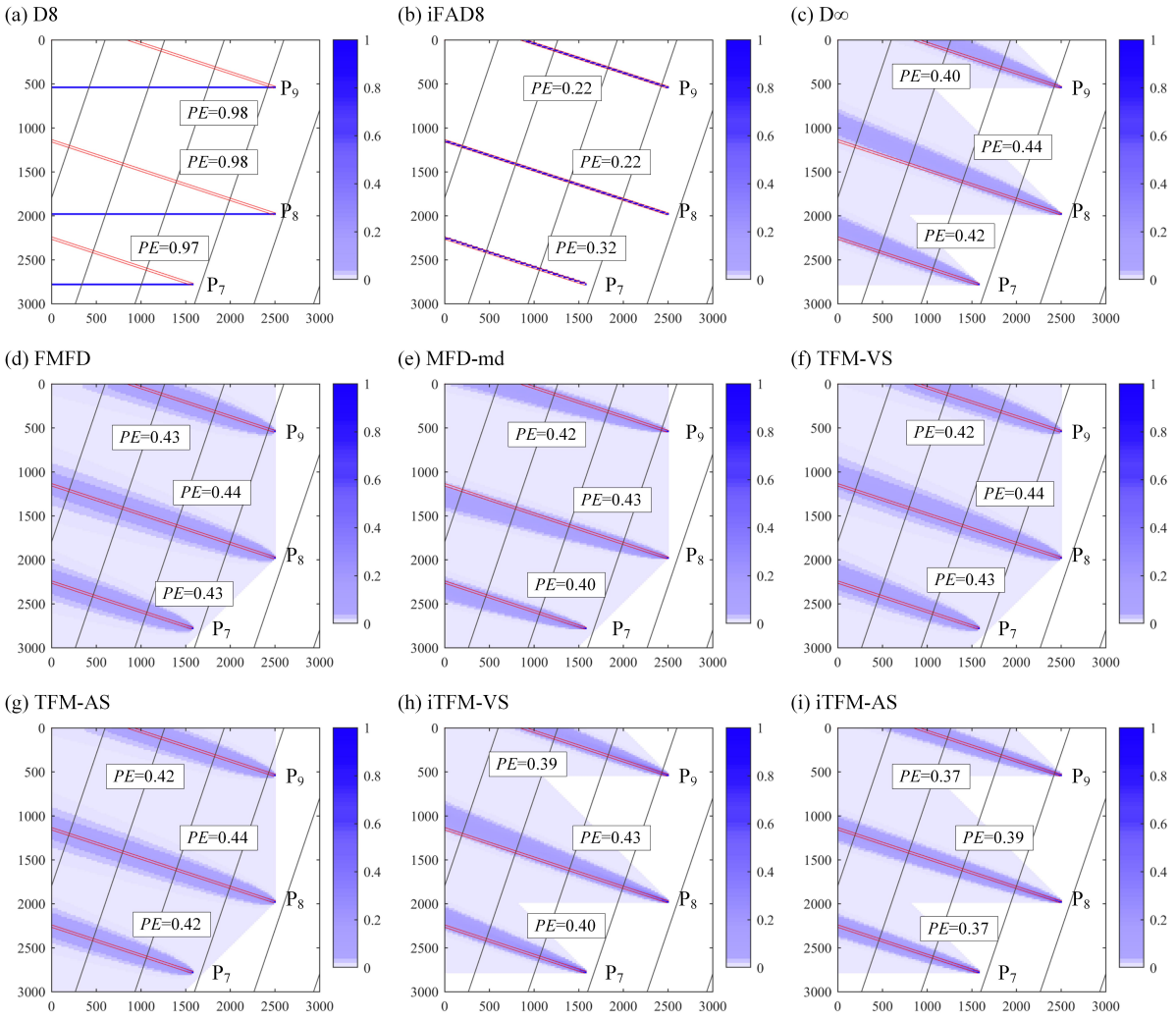

Figure 11. Extracted flow paths by different flow direction algorithms for three cells over the plane. Shades of blue represent the proportions of flow out from the source cell distributed to current cells. Contour lines have an interval of 1000 m. The coordinates of selected source cells are P_7 (1600, 2800), P_8 (2520, 2000), and P_9 (2520, 560).

Two cells (P_{10} and P_{11}) are selected over the saddle for comparison (Figure 12). P_{10} is a cell near the ridgeline, and P_{11} is a cell close to the convergent valley. The results show that D8 drains flow to false positions (Figure 12a), and the flow paths by iFAD8 overlap with the edges of the exact flow paths (Figure 12b). FMFD, MFD-md, TFM-VS and TFM-AS (Figure 12d-12g) can cause excessive artificial dispersion again. A serious problem is that a part of

the flow out of P_{10} is drained to the other side of the ridgeline. This means that water originating close to the ridge may be drained to a false catchment, which may cause essential losses and errors in hydrological/geomorphological modeling. Although D∞, iTFM-VS and iTFM-AS also cause artificial dispersion, the flow is directed to correct valleys by these algorithms. Besides, the main stream of the extracted flow path for P_{10} deviates from the exact flow path by most MFD algorithms except iTFM-VS and iTFM-AS. Similarly, the *PE*s by iTFM-VS and iTFM-AS are lower than other algorithms, and iTFM-AS outperforms iTFM-VS. Over the saddle, the *PE*s by TFM-VS and TFM-AS are lower than FMFD and MFD-md but higher than D∞.

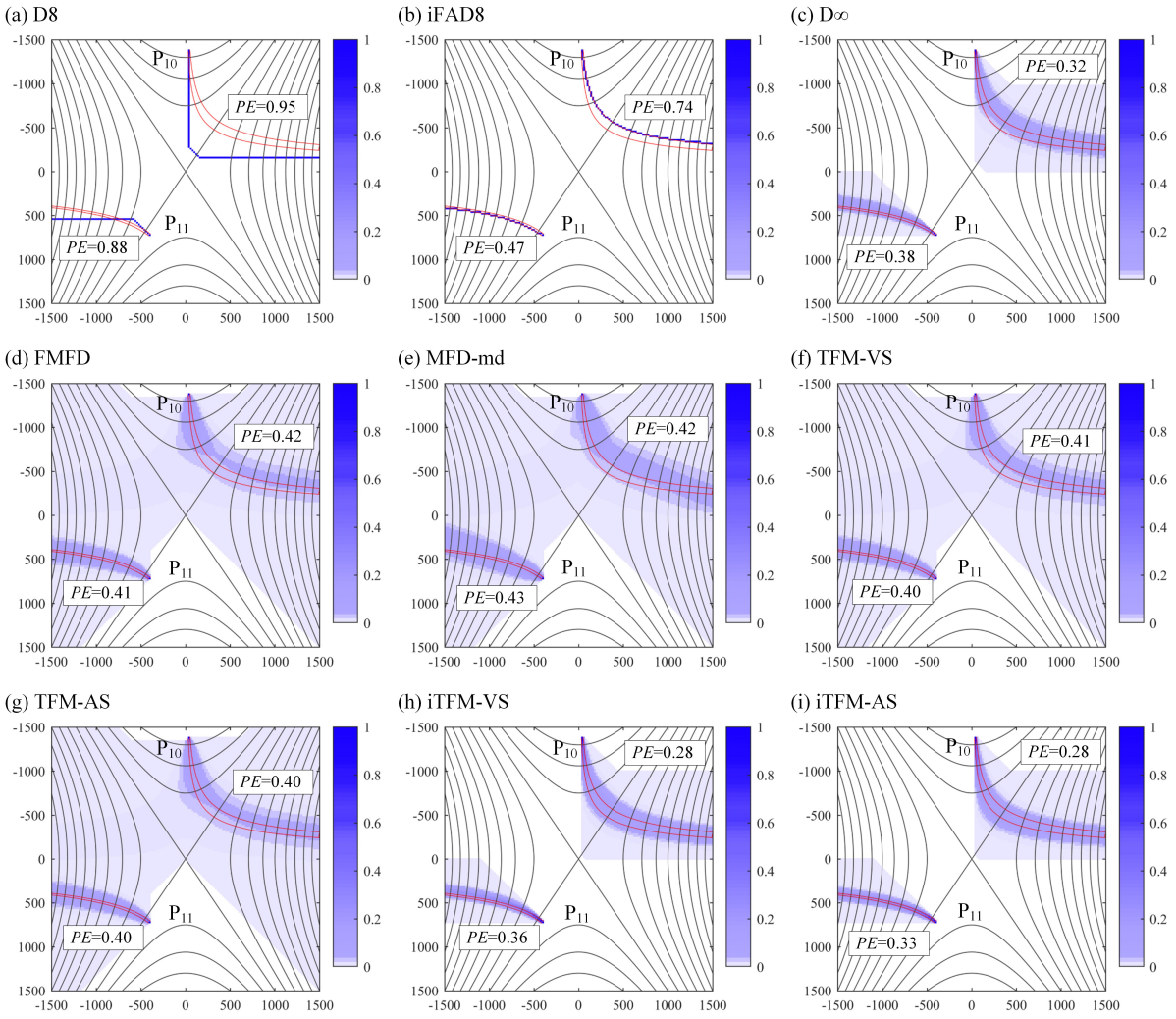

Figure 12. Extracted flow paths by different flow direction algorithms for two

cells over the saddle. Shades of blue represent the proportions of flow out from the source cell distributed to current cells. Contour lines have an interval of 25 m. The coordinates of selected source cells are P_{10} (40, -1380), and P_{11} (-400, 720).

Generally, when the 20 m-resolution DEMs are adopted, iTFM-VS and iTFM-AS ensure better position accuracy of the extracted flow paths than other algorithms according to the results in Figure 9-12, and iTFM-AS is the best one. D∞ can also limit artificial dispersion effectively. TFM-VS and TFM-AS have no superiority over other existing MFD algorithms, but TFM-AS obtains lower *PE*s than TFM-VS in more cases. Similar discovery can also be found in Table 2, which demonstrates the mean *PE* for the extracted paths of all cells within a DEM by all the flow direction algorithms. iTFM-AS and iTFM-VS are the best and the second-best algorithms based on the position accuracy on the whole, while iFAD8 only has a wonderful performance on the plane.

Table 2. Average position error (*PE*) over four artificial terrains with 20 m resolution by different flow direction algorithms

	Ellipsoid	Inverse ellipsoid	Plane	Saddle
D8	0.680	0.804	0.922	0.757
iFAD8	0.350	0.479	**0.282**	0.355
D∞	0.226	0.372	0.374	0.304
FMFD	0.318	0.422	0.402	0.374
MFD-md	0.247	0.413	0.368	0.402
TFM-VS	0.311	0.418	0.396	0.366
TFM-AS	0.309	0.417	0.393	0.364
iTFM-VS	0.226	0.369	0.361	0.288
iTFM-AS	**0.218**	**0.359**	0.338	**0.274**

Note. The lowest *PE* over every terrain within all algorithms is bolded.

The selected cells (i.e., P_1–P_{10}) in Figure 9-12 are adopted to demonstrate the influence of DEM resolutions. Figure 13 shows the change of the mean *PE* for selected cells in every terrain with different DEM resolutions. In most cases, iTFM-AS obtains lower *PE* than iTFM-VS, while TFM-AS obtains slightly lower *PE* than TFM-VS. Similar to the results in Table 2, iTFM-AS and iTFM-VS obtain the lowest and the second-lowest mean *PE*s over the ellipsoid (Figure 13a) and the saddle (Figure 13d) with nearly all five resolutions, respectively. Compared with existing algorithms, the performances of iTFM-AS and iTFM-VS are only worse than D∞ over the inverse saddle (Figure 13b) and worse than iFAD8 over the plane (Figure 13c). Furthermore, TFM-AS and TFM-VS cause relatively high PEs on all the terrains. So it can be concluded that the iTFM framework can reduce the artificial dispersion more effectively than other existing methods, and the TFM framework may cause too much artificial dispersion. In addition, AS strategy can provide better position accuracy than

VS strategy no matter iTFM or TFM framework is adopted.

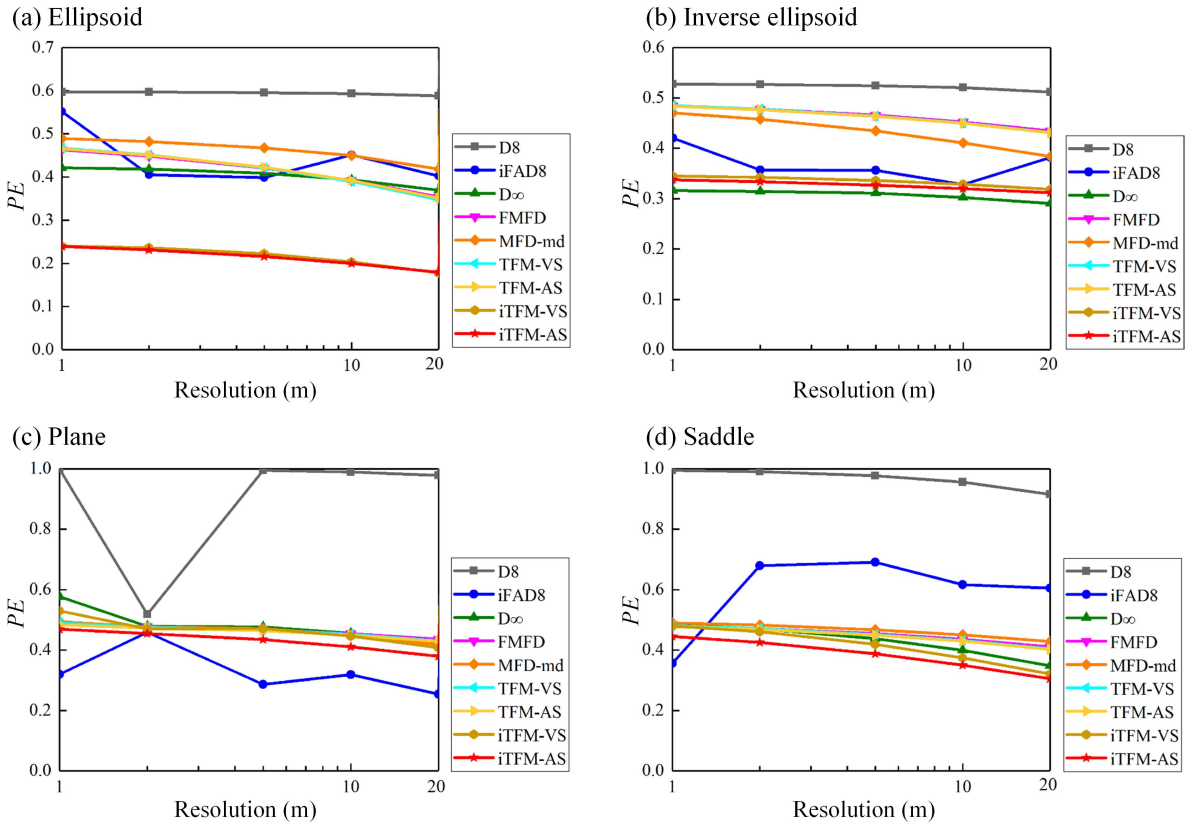

Figure 13. The mean position error (PE) of extracted flow paths for several selected cells over four artificial terrains with different resolutions derived by different flow direction algorithms.

5. Concluding remarks

A new method for dispersive flow path extraction over grid DEMs is proposed in this study. The new method (iTFM) is an improvement to the existing Triangular Form-based Multiple (TFM) Flow Direction method. In the algorithm, every cell is divided into eight triangular facets, and the flow over every facet is transferred to adjacent facets or downslope cells. In most cases, the flow draining out of a facet to downslope cells is always drained to a cardinal cell, and then is stored at the triangular facet it reaches initially in the downslope cell as shown in Figure 2. Subsequently, two common strategies including vector split (VS) and area split (AS) are adopted to split the flow over a facet into two parts. Four algorithms (i.e., TFM-VS, TFM-AS, iTFM-VS and iTFM-AS) are

generated for assessment by combining different frameworks and split strategies.

The algorithms above are compared with two existing SFD algorithms (D8 and iFAD8) and three existing MFD algorithms (D∞, FMFD and MFD-md) over four artificial terrains. Both the capacity to reproduce the theoretical TCA and the position accuracy of extracted flow paths are adopted as assessment criteria. The results show that iTFM-VS and iTFM-AS can provide the estimated TCAs with fewer deviations than other algorithms over any terrain with any resolution ranging from 1 m to 40 m. iTFM-VS and iTFM-AS can also extract flow paths closer to the exact ones than other algorithms. Besides, the errors of the estimated TCAs by TFM-VS and TFM-AS are similar to FMFD, and less than the other four existing algorithms in most cases. But the position accuracy of the extracted flow paths by TFM-VS and TFM-AS have no advantage over other existing MFD algorithms. Hence, the proposed iTFM framework is an effective improvement to the existing TFM framework and is more accurate than other existing algorithms. In addition, iTFM-AS has a better performance than iTFM-VS, while TFM-AS is more accurate than TFM-VS in most cases. This phenomenon indicates that AS strategy is more suitable than VS strategy for flow split within a triangular facet. Overall, the iTFM-AS algorithm has a high potential for dispersive flow path extraction.

Acknowledgements

This work was supported by the National Natural Science Foundation of China (NSFC; grant nos. 92047301, 41771025 and 41730750). The authors would like to thank Petter Pilesjö and Abdulghani Hasan (Lund University) for the MATLAB codes of TFM. The Java codes of all the drainage direction algorithms used in this study are available at: https://github.com/hhuwpf/iTFM, and the data of artificial terrains are available at: https://doi.org/10.6084/m9.figshare.16909321.v1.

References

Beven, K. J., & Kirkby, M. J. (1979). A physically based, variable contributing area model of basin hydrology. *Hydrological Sciences Bulletin*, 24(1), 43-69. https://doi.org/10.1080/02626667909491834

Bonetti, S., Bragg, A. D., & Porporato, A. (2018). On the theory of drainage area for regular and non-regular points. *Proceedings of the Royal Society A: Mathematical, Physical and Engineering Sciences*, 474, 20170693. https://doi.org/10.1098/rspa.2017.0693

Bonetti, S., Hooshyar, M., Camporeale, C., & Porporato, A. (2020). Channelization cascade in landscape evolution. *Proceedings of the National Academy of Sciences of the United States of America*, 117(3), 1375-1382. https://doi.org/10.1073/pnas.1911817117

Costa-Cabral, M. C., & Burges, S. J. (1994). Digital elevation model networks (DEMON): A model of flow over hillslopes for computation of contributing and dispersal areas. *Water Resources Research*, 30(6), 1681-1692. https://doi.org/10.1029/93WR03512

Fairfield, J., & Leymarie, P. (1991). Drainage networks from grid digital elevation models. *Water Resources Research*, 27(5), 709-717. https://doi.org/10.1029/90WR02658

Freeman, T. G. (1991). Calculating catchment area with divergent flow based on a regular grid. *Computers & Geosciences*, 17(3), 413-422. https://doi.org/10.1016/0098-3004(91)90048-I

Holmgren, P. (1994). Multiple flow direction algorithms for runoff modelling in grid based elevation models: an empirical evaluation. *Hydrological Processes*, 8, 327-334. https://doi.org/10.1002/hyp.3360080405

Hooshyar, M., Wang, D., Kim, S., Medeiroset, S. C., & Hagen, S. C. (2016). Valley and channel networks extraction based on local topographic curvature and k-means clustering of contours. *Water Resources Research*, 52, 8081-8102. https://doi.org/10.1002/2015WR018479

Kotyra, B., Chabudziński, Ł., & Stpiczyński, P. (2021). High-performance parallel implementations of flow accumulation algorithms for multicore architectures. *Computers & Geosciences*, 151, 104741. https://doi.org/10.1016/j.cageo.2021.104741

Lea, N. L. (1992). An aspect driven kinematic routing algorithm. In A. J. Parsons & A. D. Abrahams (Eds.), *Overland Flow: Hydraulics and Erosion Mechanics* (pp. 393-407). New York: Chapman and Hall.

Li, Z., Yang, T., Wang, C., Shi, P., Yong, B., & Song, Y. (2021). Assessing the precision of total contributing area (TCA) estimated by flow direction algorithms based on the analytical solution of theoretical TCA on synthetic surfaces. *Water Resources Research*, 57, e2020WR028546. https://doi.org/10.1029/2020WR028546

Li, Z., Yang, T., Xu, C. Y., Shi, P., & Wang, C. (2020). Evaluating the area and position accuracy of surface water paths obtained by flow direction algorithms. *Journal of Hydrology*, 583, 124619. https://doi.org/10.1016/j.jhydrol.2020.124619

Lindsay, J. B. (2003). A physically based model for calculating contributing area on hillslopes and along valley bottoms. *Water Resources Research*, 39, 291-297. https://doi.org/10.1029/2003WR002576

Liu, J., Chen, X., Lin, H., Liu, H., & Song, H. (2013). A simple geomorphic-based analytical model for predicting the spatial distribution of soil thickness in headwater hillslopes and catchments. *Water Resources Research*, 49, 7733-7746. https://doi.org/10.1002/2013WR013834

Maxwell, J. C. (1870). On hills and dales. *The London, Edinburgh, and Dublin Philosophical Magazine and Journal of Science*, 40(269), 421-427.

Moore, I. D., Gessler, P. E., Nielsen, G. A., & Peterson, G. A. (1993). Soil attribute prediction using terrain analysis. *Soil Science Society of America Journal*, 57(2), 443-452. https://doi.org/10.2136/sssaj1993.572NPb

Moore, I. D., & Grayson, R. B. (1991). Terrain-based catchment partitioning and runoff prediction using vector elevation data. *Water Resources Research*, 27(6), 1177-1191. https://doi.org/10.1029/91WR00090

Nilsson, H., Pilesjö, P., Hasan, A., & Persson, A. (2021). Dynamic spatio-temporal flow modeling with raster DEMs. *Transactions in GIS*, 00, 1-17. https://doi.org/10.1111/tgis.12870

O'Callaghan, J. F., & Mark, D. M. (1984). The extraction of drainage networks from digital elevation data. *Computer Vision, Graphics, and Image Processing*, 28(3), 323-344. https://doi.org/10.1016/S0734-189X(84)80011-0

Orlandini, S., & Moretti, G. (2009). On the determination of surface flow paths from gridded elevation data. *Water Resources Research*, 45, W03417. https://doi.org/10.1029/2008WR007099

Orlandini, S., Moretti, G., Corticelli, M. A., Santangelo, P. E., Capra, A., Rivola, R., & Albertson, J. D. (2012). Evaluation of flow direction methods against field observations of overland flow dispersion. *Water Resources Research*, 48, W10523. https://doi.org/10.1029/2012WR012067

Orlandini, S., Moretti, G., Franchini, M., Aldighieri, B., & Testa, B. (2003). Path-based methods for the determination of nondispersive drainage directions in grid-based digital elevation models. *Water Resources Research*, 39(6), 1144. https://doi.org/10.1029/2002WR001639

Orlandini, S., Moretti, G., & Gavioli, A. (2014). Analytical basis for determining slope lines in grid digital elevation models. *Water Resources Research*, 50, 526-539. https://doi.org/10.1002/2013WR014606

Pan, F., Stieglitz, M., & Mckane, R. B. (2012). An algorithm for treating flat areas and depressions in digital elevation models using linear interpolation. *Water Resources Research*, 48, 229-235. https://doi.org/10.1029/2011WR010735

Paik, K. (2008). Global search algorithm for nondispersive flow path extraction. *Journal of Geophysical Research*, 113, F04001. https://doi.org/10.1029/2007JF000964

Pilesjö, P., & Hasan, A. (2014). A triangular form-based multiple flow algorithm to estimate overland flow distribution and accumulation on a digital elevation model. *Transactions in GIS*, 18(1), 108-124. https://doi.org/10.1111/tgis.12015

Pilesjö, P., Zhou, Q., & Harrie, L. (1998). Estimating flow distribution over digital elevation models using a form-based algorithm. *Geographic Information Sciences*, 4(1-2), 44-51. https://doi.org/10.1080/10824009809480502

Planchon, O., & Darboux, F. (2002). A fast, simple and versatile algorithm to fill the depressions of digital elevation models. *Catena*, 46(2-3), 159-176. https://doi.org/10.1016/S0341-8162(01)00164-3

Qin, C. Z., Bao, L. L., Zhu, A. X., Hu, X. M., & Qin, B. (2013). Artificial surfaces simulating complex terrain types for evaluating grid-based flow direction algorithms. *International Journal of Geographical Information Science*, 27(6), 1055-1072. http://doi.org/10.1080/13658816.2012.737920

Qin, C., Zhu, A. X., Pei, T., Li, B., Zhou, C., & Yang, L. (2007). An adaptive approach to selecting a flow-partition exponent for a multiple-flow-direction algorithm. *International Journal of Geographical Information Science*, 21(4), 443-458. https://doi.org/10.1080/13658810601073240

Quinn, P., Beven, K., Chevallier, P., & Planchon, O. (1991). The prediction of hillslope flow paths for distributed hydrological modelling using digital terrain models. *Hydrological Processes*, 5, 59-79. https://doi.org/10.1002/hyp.3360050106

Quinn, P. F., Beven, K., & Lamb, R. (1995). The $\ln(a/\tan)$ index: How to calculate it and how to use it within the TOPMODEL framework. *Hydrological Processes*, 9(2), 161-182. https://doi.org/10.1002/hyp.3360090204

Seibert, J., & McGlynn, B. L. (2007). A new triangular multiple flow direction algorithm for computing upslope areas from gridded digital elevation models. *Water Resources Research*, 43, W04501. https://doi.org/10.1029/2006WR005128

Shin, S., & Paik, K. (2017). An improved method for single flow direction calculation in grid digital elevation models. *Hydrological Processes*, 31(8), 1650-1661. https://doi.org/10.1002/hyp.11135

Tarboton, D. G. (1997). A new method for the determination of flow directions and upslope areas in grid digital elevation models. *Water Resources Research*, 33(2), 662-670. https://doi.org/10.1029/96WR03137

Vivoni, E. R., Ivanov, V. Y., Bras, R. L., & Entekhabi, D. (2005). On the effects of triangulated terrain resolution on distributed hydrologic model response. *Hydrological Processes*, 19, 2101-2122. https://doi.org/10.1002/hyp.5671

Wilson, J. P.& Gallant, J. C. (Eds.), (2000). *Terrain analysis: Principles and applications*. New York: John Wiley & Sons.

Wilson, J. P., Lam, C. S., & Deng, Y. (2007). Comparison of the performance of flow-routing algorithms used in GIS-based hydrologic analysis. *Hydrological Processes*, 21, 1026-1044. https://doi.org/10.1002/hyp.6277

Wu, P., Liu, J., Han, X., Liang, Z., Liu, Y., & Fei, J. (2020). Nondispersive drainage direction simulation based on flexible triangular facets. *Water Resources Research*, 55, e2019WR026507. https://doi.org/10.1029/2019WR026507

Yamazaki, D., Ikeshima, D., Sosa, J., Bates, P. D., Allen, G. H., & Pavelsky, T. M. (2019). MERIT hydro: A high-resolution global hydrography map based on latest topography dataset. *Water Resources Research*, 55, 5053-5073. https://doi.org/10.1029/2019WR024873

Yan, Y., Tang, J., & Pilesjo, P. (2018). A combined algorithm for automated

drainage network extraction from digital elevation models. *Hydrological Processes*, 32, 1322-1333. https://doi.org/10.1002/hyp.11479

Zhou, Q., & Liu, X. (2002). Error assessment of grid-based flow routing algorithms used in hydrological models. *International Journal of Geographical Information Science*, 16(8), 819-842. https://doi.org/10.1080/13658810210149425

Zhou, Q., Pilesjö, P., & Chen, Y. (2011). Estimating surface flow paths on a digital elevation model using a triangular facet network. *Water Resources Research*, 47, W07522. https://doi.org/10.1029/2010WR009961